Journal of Marine Research, 64, 853–880, 2006

Variability in the Indian Ocean circulation and salinity and its impact on SST anomalies during dipole events

by Bijoy Thompson[1], C. Gnanaseelan[1,2] and P. S. Salvekar[1]

ABSTRACT

The GFDL Modular Ocean Model (MOM4) has been used to understand the variability of the Indian Ocean circulation and salinity during Indian Ocean Dipole events. The model simulations are compared with HadISST, SODA and ECCO data sets. During the positive dipole years, the climatological cyclonic circulation in the Bay of Bengal weakens or is replaced by an anticyclonic circulation. The interannual variability in the Wyrtki Jet and Bay of Bengal circulation has significant influence on fresh water transport between the equatorial Indian Ocean and Bay of Bengal. The salinity anomalies in the equatorial Indian Ocean are significant during the positive dipole years. The salinity anomalies are positive in the southeastern equatorial Indian Ocean and negative in the central equatorial Indian Ocean. The advection of low salinity water from the eastern equatorial Indian Ocean and Bay of Bengal is attributed to the salinity anomalies in the central equatorial Indian Ocean. The salinity variability in the equatorial Indian Ocean influences the surface and subsurface temperatures by forming or eroding the barrier layer.

1. Introduction

Increased precipitation over tropical eastern Africa and the western Indian Ocean along with severe drought over Indonesia during 1961 and 1997–1998 (Saji *et al*., 1999; Webster *et al.,* 1999) motivated atmospheric and oceanic researchers to extensively investigate the thermodynamic and dynamic processes of the tropical Indian Ocean. In the climatological scenario, the eastern part of the Equatorial Indian Ocean (EIO) is warmer than the western part. However, the anomalous patterns of Sea Surface Temperature (SST) gradients were observed in the equatorial Indian Ocean during the Indian Ocean Dipole (IOD) years (Saji *et al*., 1999). In addition to the reversal of the SST gradient, the weak equatorial westerly winds were also replaced by easterly winds (Webster *et al*., 1999). Masson *et al.* (2002) and several others observed that during October and November 1997, the equatorial Indian Ocean was marked by a westward wind stress of 0.2 N/m^2–0.3 N/m^2, resulting in anomalous cooling in the east and warming in the western EIO. In contrast, 1996 is characterised by positive SST anomalies in the Southeastern Tropical Indian Ocean (STIO) and negative SST anomalies in the western EIO. These unusual warming (cooling) events

1. Indian Institute of Tropical Meteorology, Dr. Homibhabha Road, Pune 411008, India.
2. Corresponding author: ***email: seelan@tropmet.res.in***

in the western equatorial Indian Ocean and cooling (warming) events in the STIO are referred to as positive (negative) IOD events (Saji *et al*., 1999; Webster *et al*., 1999). These SST anomalies represent one of the dominant modes of basin scale SST variability in the Indian Ocean. The variability in the Indian Ocean SST is extensively discussed by Nicholls (1989); Behera *et al.* (1999 and 2000); Murtugudde and Busalachi (1999); Murtugudde *et al.* (2000); Iizuka *et al.* (2000), and Vinayachandran *et al.* (2002). The impact of IOD on the climate of the region around the Indian Ocean is widely described in Zubair *et al.* (2003), Behera and Yamagata (2003), and Saji and Yamagata (2003). There are many studies in the recent past focusing on the relationship between IOD and east African rain fall. Behera *et al.* (2005) showed that the influence of the IOD on east African short rains is dominant over the El Niño/Southern Oscillation. Rao *et al.* (2002a) and Rao and Behera (2005) examine the subsurface temperature variability in the Indian Ocean during the IOD events using observational data and Ocean General Circulation Model (OGCM) simulations.

The presence of a thick barrier layer in the east equatorial Indian Ocean is reported by Sprintall and Tomczak (1992), Godfrey *et al.* (1999), and Masson *et al.* (2002). The generation and survival of this barrier layer largely depend on the intrusion of the eastward flowing equatorial jet (Wyrtki Jet) into the east equatorial Indian Ocean (Masson *et al*., 2002; 2003). The variability in the barrier layer influences the formation and growth of IOD events. The absence of the barrier layer off the Sumatra coast during the positive IOD events aids the cooling of SSTs via the Sumatra upwelling (Murtugudde *et al*., 2000; Annamalai *et al*., 2003; Masson *et al.,* 2004). Masson *et al.* (2002) show the importance of salinity and water mass transport during the IOD years. The anomalous equatorial Indian Ocean circulations that evolve during IOD events influence SST in the region through strong Barrier Layer Thickness (BLT) anomalies.

Considerable changes in the equatorial Indian Ocean circulation were observed when strong wind anomalies persisted during the dipole mode years. Murtugudde *et al.* (2000) discuss the reversal of Wyrtki Jet and subsurface current variability during the boreal fall of 1997. Grodsky *et al.* (2001), using observational data from surface drifters study the anomalous circulation pattern in the equatorial Indian Ocean during the anomalous climatic events of 1994 and 1997. Their study shows the importance of a momentum balance between the wind-induced momentum flux and the pressure gradient force, as well as the role of horizontal temperature advection in the upper ocean thermodynamics of the equatorial Indian Ocean. Using an OGCM, Vinayachandran *et al.* (2002) also finds that the Wyrtki Jets were weak or absent during the positive IOD years of 1994 and 1997. They also show that the strong anomalous easterly winds are responsible for the westward currents along the equatorial Indian Ocean in 1997 and the weakening of the Wyrtki Jets during the 1994 dipole periods. However, a detailed analysis exploring the surface and subsurface circulation variability in the EIO is essential in understanding the ocean dynamics and their influence on SST variability over this region. Previous studies found

that the anomalous circulation pattern in the EIO has a remarkable impact on the surface and subsurface temperature anomalies during IOD years (Masson *et al.,* 2002; 2004).

The variability in the circulation and salinity transports over the Bay of Bengal (BoB) during the IOD events are not well described in the literature. Rao *et al.* (2002b) discuss the mechanisms responsible for the absence of cool SST anomalies in the BoB during the 1997 IOD event. Their study shows that despite the northward propagation of upwelling Kelvin waves in the bay, the presence of a highly stratified, near surface pool of fresh water prevented the SST cooling through internal ocean dynamics. Jensen (2006), using a 4.5 layer model, examines water mass exchanges between the Arabian Sea and BoB during El Nino, La Nina, and IOD events. The study concludes that transport from the Arabian Sea (BoB) to BoB (Arabian Sea) is enhanced (decreased) during El Nino and IOD years. Shaji *et al.* (2003) discuss the seasonal evolution of the salinity field in the Arabian Sea and Bay of Bengal using OGCM simulation. The variability in the northern Indian Ocean Sea Surface Salinity (SSS) and mixed layer salinity budget are addressed in Rao *et al.* (2003). A detailed study of the salinity transport between the BoB and equatorial Indian Ocean during the IOD events is not available in the literature.

The objective of this paper is to understand the interannual variability of the circulation pattern in the EIO and Bay of Bengal during IOD events, the influence of the anomalous circulation pattern on the salinity and barrier layer thickness anomalies and the possible influence of the salinity and barrier layer thickness anomalies on the SST variability during IOD years. The present analysis is based on the simulations from an OGCM for the period 1958–2000. The circulation and salinity variability during the strong positive IOD years (1961, 1963, 1967, 1972, 1982, 1994, and 1997) and negative IOD years (1958, 1960, 1975, 1984, 1992, and 1996) are discussed in this study. The analysis of the model currents shows strong interannual variability in the surface and subsurface circulation in the EIO and BoB during the positive IOD years. The anomalous circulations during individual positive IOD years are analyzed in this paper. However, the salinity and barrier layer thickness anomalies show similar patterns of varying magnitudes during all the positive (or negative) IOD years. The analogous spatial pattern of salinity and barrier layer anomalies during IOD years allowed us to perform a composite analysis to understand their interannual variability.

2 Model, methodology and datasets

The Ocean General Circulation Model used for the present study is the Geophysical Fluid Dynamics Laboratory (GFDL) Modular Ocean Model Version 4 (MOM4p0c) (Griffies *et al*., 2003). MOM is a z–coordinate, free surface ocean general circulation model. The model domain is 30E to 120E and 40S to 25N with 30 vertical levels. The upper 150 m has 10 m vertical resolution, and the thickness gradually increases to a maximum of 712 m at 5200 m. The model has a constant zonal resolution of 1^{o} and a meridional resolution varying from 0.3353^{o} at the equator to 0.7^{o} at 25N and 1.5^{o} at 40S. Realistic bottom topography of 0.5^{o} resolution is provided to the model. Sponge layers of

4° thickness are applied in the eastern and southern boundaries where model temperatures and salinities are relaxed towards Levitus (1998) monthly climatology. The model is initialized with annual climatologies of temperature and salinity from Levitus (1998) and forced with climatological short wave and long wave radiation, 10m wind fields, specific humidity, air temperature and surface precipitation from NCAR climatology. Chlorophyll-*a* climatology computed from SeaWiFS satellite for the period 1999–2001 is provided to handle short wave penetration. After 20 years of spin up, the model is integrated for a period of 43 years from 1958–2000 with the NCAR corrected interannual datasets (Large and Yeager, 2004) of daily downwelling shortwave and longwave radiation, 10 m wind fields, specific humidity, air temperature, and monthly precipitation. During the interannual simulation, the surface fluxes are corrected on a 30-day timescale using seasonal climatological sea surface temperature and sea surface salinity. The basin wide average of this correction term during the simulation period for heat flux is in the range -6 W/m^2 to 8 W/m^2, and the fresh water flux is in the range -2.5×10^{-9} to 0.5×10^{-9} m/s. The 43 year mean of heat flux correction shows 84% of the area of the basin within the range ± 5 W/m^2 and 10% of the area within the range -5 to -7 W/m^2 and 5 to 7 W/m^2. The head bay, western Arabian Sea, and Madagascar area show the flux correction of about ± 5 W/m^2. The heat flux correction above 10 W/m^2 is seen only in the Persian Gulf. For the fresh water flux 85% of the area of the basin shows a correction of less than $\pm 0.2 \times 10^{-7}$ m/s and 12% area in the range -0.2 to -0.5×10^{-7} m/s and 0.2 to 0.5×10^{-7} m/s. Fresh water flux corrections above $\pm 0.2 \times 10^{-7}$ m/s are seen in the east and west BoB regions. These low values of flux corrections show that the model interannual simulations are not significantly affected by the weak SST and SSS restoring terms.

The Hadley Center Ice Sea Surface Temperature (HadISST v.1.1) (Rayner *et al*., 2003), the Simple Ocean Data Assimilation (SODA_1.4.2) data and Estimating Climate and Circulation of the Ocean (ECCO) data are used for model calibration and comparison. The SODA and ECCO assimilation procedures are explained in Carton *et al.* (2000 and 2005) and Kohl *et al.* (2003), respectively.

The difference in depth between the bottom of the isothermal layer and the bottom of the mixed layer is defined as the barrier layer thickness. The isothermal layer is defined as the depth where the temperature differs from SST by 0.5°C. The mixed layer is defined as the depth where density differs from the surface density by 0.125 kg/m^3.

3. Results and discussion

a. SST variability during IOD events

The intensity of IOD events can be represented with a simple time series index called Dipole Mode Index (DMI). Saji *et al.* (1999) define DMI as the difference between the SST anomalies in the western equatorial Indian Ocean (50E to 70E, 10S to 10N, hereafter the western basin) and the southeastern tropical Indian Ocean (90E to 110E, 10S to the Equator, hereafter the eastern basin). The DMI derived from the model, HadISST, and

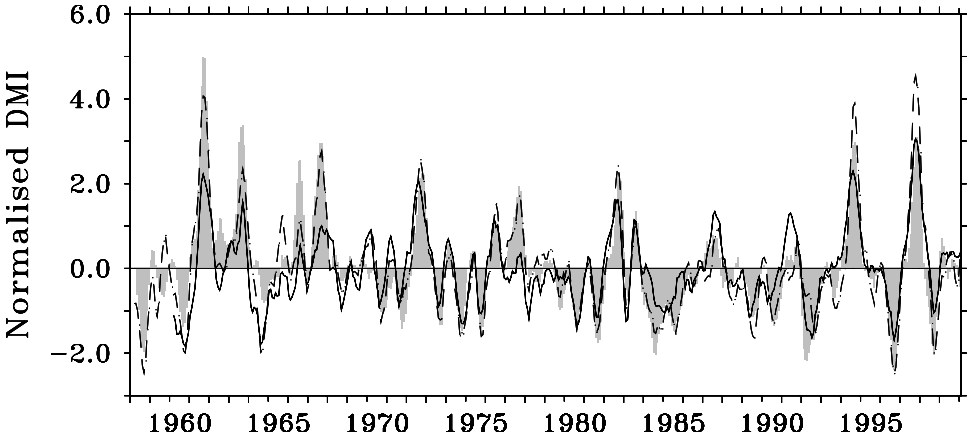

Figure 1. Dipole mode Index time series. Model (shaded), HadISST (continuous line), SODA (dashed line).

SODA data sets are shown in Figure 1. The model has simulated the recent positive IOD events (1961, 1963, 1967, 1972, 1977, 1982, 1994 and 1997) and negative IOD events (1958, 1960, 1964, 1975, 1984, 1989, 1992 and 1996) very well. The model DMI compares very well with the DMI calculated from HadISST. Considerable differences with the DMI are seen in 1961 and 1963. For 1961, both the model and SODA overestimate the DMI. The peak phases of eastern cooling are observed in October during 1961 and 1994; whereas, the peak cooling was in November during 1997 (figure not shown, similar features are observed by Vinayachandran *et al*., 2002). The model simulation of eastern cooling is more than 2°C in 1961; whereas, the cooling is only 1.5°C in HadISST. Both the model and observation show basinwide warming (of about 0.8°C) in the western equatorial Indian Ocean and cooling (of about 2°C) in the southeastern equatorial Indian Ocean during November 1997.

b. Simulation of North Indian Ocean circulation

The model climatological surface currents for February, May, July and November are shown in the left panel of Figure 2, and the corresponding SODA currents are shown in the right panel of Figure 2. The North Indian Ocean is subjected to unique seasonally reversing winds. The westward flowing winter monsoon current or North East Monsoon Current (NEMC) is observed between 2S and 5N from 90E up to the African coast during this season. The NEMC reaches its maximum strength of about 0.65 m/s near 65E. Along the African coast, a major portion of the NEMC flows southward and forms the Somali Current. During the southwest monsoon season, the Somali Current reverses its direction and flows northward. The eastward flowing north equatorial current joins with the West Indian Coastal Current (which flows southward along the west coast of India) south of Sri Lanka, forming the South West Monsoon Current (SWMC). The SWMC shows a

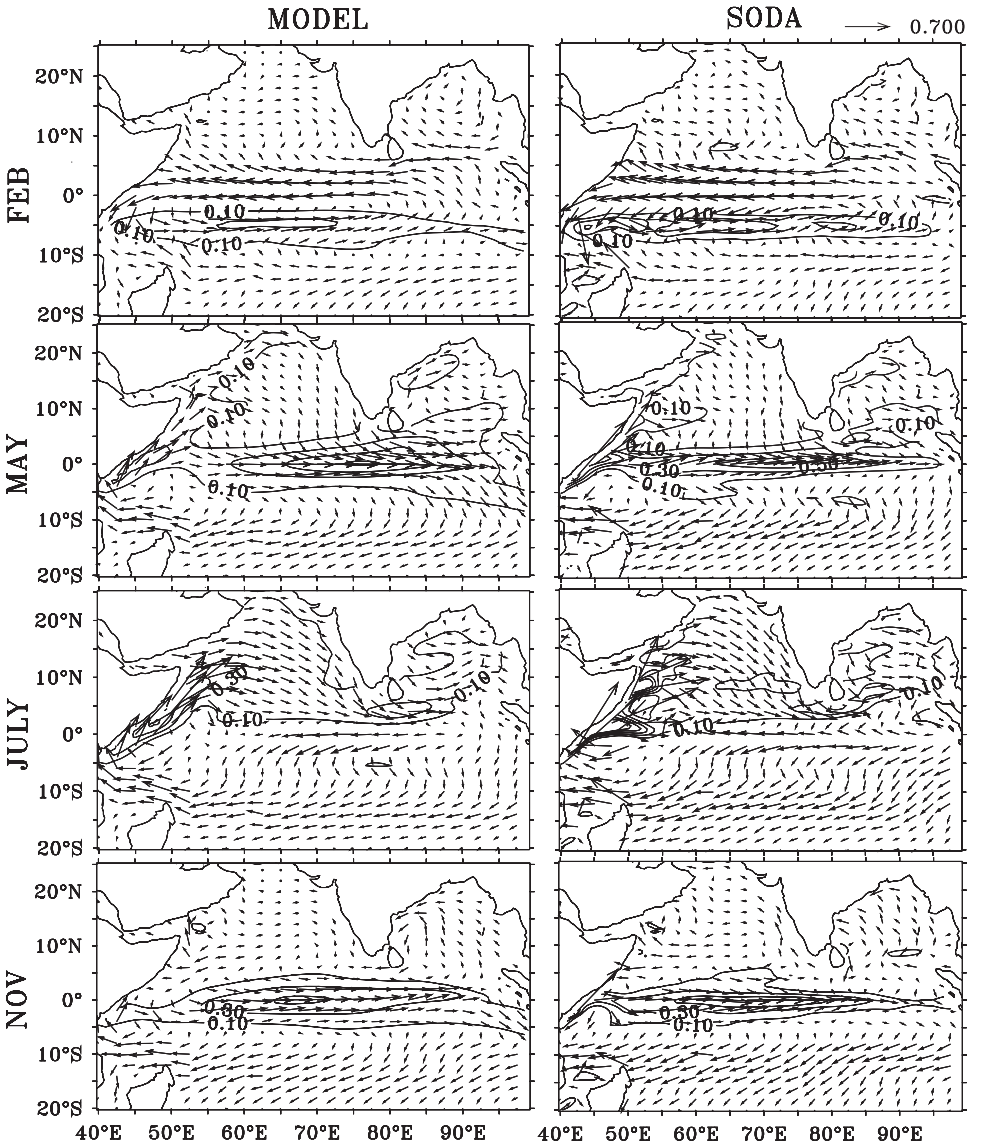

Figure 2. Surface Current (m/s) Climatology (1958-2000) from Model (left) and SODA (right) for February, May, July and November. Contours represent Zonal eastward currents.

maximum strength of about 0.4 m/s near 5N, 85E. The Indian Ocean south of 10S, where easterly winds persist throughout the year, is less influenced by the seasonal reversal of winds. The model simulations show the existence of the westward flowing South Equatorial Current (SEC) south of 10S, during the entire year (without much intrannual

variability). The SEC shows a maximum strength of 0.15 m/s during the boreal winter and 0.2 m/s during the boreal summer.

The equatorial Indian Ocean circulation is marked by the semiannual occurrence of eastward Wyrtki Jets during the monsoon transition periods of April/May and October/November, which are well simulated by the model. However, during February and August, westward currents prevail in the EIO. These westward currents show a maximum strength of about 0.65 m/s in February near 65E and about 0.4 m/s in July near 70E. The Wyrtki Jet, simulated by the model during the boreal spring season shows magnitudes of about 0.7 m/s between 70E and 80E, and the boreal fall jets have magnitudes of about 0.55 m/s between 60E to 70E. However the observations show jet magnitudes of about 0.8 m/s during boreal spring and 0.9 m/s during boreal fall. Recently, Han *et al.* (1999) and Schott and MacCreary (2001) demonstrate the weakening of fall jets in the OGCM simulations. In general, the spatial pattern of the model jets agrees very well with the observations.

The model simulation of surface currents in the north Indian Ocean shows good agreement with earlier studies such as Reverdin (1987), Hastenrath and Greischar (1991), Han *et al.* (1999), Schott and McCreary (2001) and Masson *et al.* (2002). The model's ability to reproduce the climatological circulation in the Indian Ocean has encouraged the authors to do more analysis on understanding the interannual variability in the North Indian Ocean circulation pattern. Since the ECCO data sets are available only since 1992, the model simulations are compared with ECCO simulations for 1994, 1996 and 1997 IOD events. For all the events prior to 1992, model simulations are compared to SODA datasets.

c. Anomalous equatorial Indian Ocean circulation

Unlike the Pacific and Atlantic oceans, the north equatorial current reverses its direction and flows eastward during the summer (boreal) monsoon season. This feature constitutes the SWMC, and it persists until September-October. By December, the North Equatorial Current (NEC) flows westward, with an eastward-flowing equatorial counter current existing south of the equator. A different anomalous circulation pattern is observed during the positive IOD years. A strong westward current is seen from 10S to 2.5N during October 1961 (figure not shown). The north equatorial current weakens and is confined to a narrow band north of 2.5N. Around 85E the NEC turns northward to the east of Sri Lanka. Even though the Wyrtki Jet appears in November 1961, the jet has a discontinuous pattern over 75E-85E. During 1963, the jet is present in October, but the current pattern is completely disturbed between 75E-85E during November. A disintegrated current pattern is seen in the EIO during 1967. In October, strong eastward currents west of 75E and southwestward currents east of 85E are seen in the EIO. The jet appears east of 85E as a narrow band in November. A part of the jet turns northward and flows northeastward around 70E (figures not shown). During October 1972, eastward currents are seen in the region west of 70E and from the equator to 5N, while westward currents prevail in the region east of 70E and between 5S and the equator. By November the westward currents push the eastward currents (jet) farther north of 2.5N; consequently, the jet bifurcates into a northward

flowing branch and a narrow band of eastward current along 2.5N. A similar pattern of circulation is seen during October 1982 also. However, in November at 75E, the eastward currents split into three branches, flowing a southward, eastward, and northward. During 1994, the eastward flow is seen in the region west of 80E and from the equator to 5N, whereas the westward current is dominant in the region east of 70E and south of the equator. Another important feature in the circulation pattern is the weakened Wyrtki Jet near 75-80E, which resulted in the western part of the jet taking a cyclonic turn in the northern hemisphere (figures not shown). During October and November 1997, strong westward currents are seen in the EIO. Figures 3 and 4 represent the model simulated and ECCO surface currents for October 1996 to January 1997 and October 1997 to January 1998, respectively. Westward zonal current anomalies of more than 1 m/s are observed between 70E and 75E over the EIO during October 1997. In November the zonal current anomaly becomes slightly weaker in magnitude (0.9 m/s) but the region of maximum current anomaly extends further west to 60E. The anomalous wind forcing observed over the equatorial Indian Ocean (Saji *et al*., 1999; Webster *et al*., 1999; Vinayachandran *et al*., 1999b) is one of the dominant factors, which causes the strong variability in the equatorial Indian Ocean circulation. The anomaly composites of surface current and wind stress over the tropical Indian Ocean during the peak IOD phase (October-November) for the strong positive IOD years 1961, 1994 and 1997 are shown in Figure 5. Strong westward current anomalies are seen in the anomaly composite. Corresponding to the current anomalies, strong westward wind stress anomalies are also observed over the equatorial Indian Ocean (Fig. 5). The co-occurrence of strong westward current anomalies in the EIO along with strong wind stress anomalies indicates the strong influence of wind stress in forcing anomalous surface currents. The momentum budget of equatorial Indian Ocean discussed later in this section clearly shows the significance of these wind anomalies in driving the upper ocean currents during the anomalous years. In negative IOD years the EIO maintains a circulation pattern similar to the climatological one, but the Wyrtki Jet and southwest monsoon currents are intense during all the negative IOD years considered in this study. Positive zonal current anomalies of about 0.4 m/s are seen in the EIO during October and November 1996.

The pattern of the upper layer circulation in the Indian Ocean changes during the positive IOD years and shows some resemblance to Pacific and Atlantic Ocean circulation patterns. The EIO is characterised by strong westward currents during October and November 1997. These westward currents intrude up to a depth of 50 m. Strong eastward currents are seen below 50 m (Fig. 6). The maximum intensity of eastward currents is observed in the region 80E to 90E at a depth of around 80 m, where the maximum anomalous cooling is observed. The circulation pattern of westward currents in the upper layer and eastward currents in the subsurface during the positive IOD years establishes a vertical-zonal circulation in the EIO (Fig. 7). The upward vertical advection of cold subsurface water (Fig. 8) leads to the formation of negative temperature anomalies in the STIO. The weakening of the Wyrtki Jet or the westward current aids this cooling by

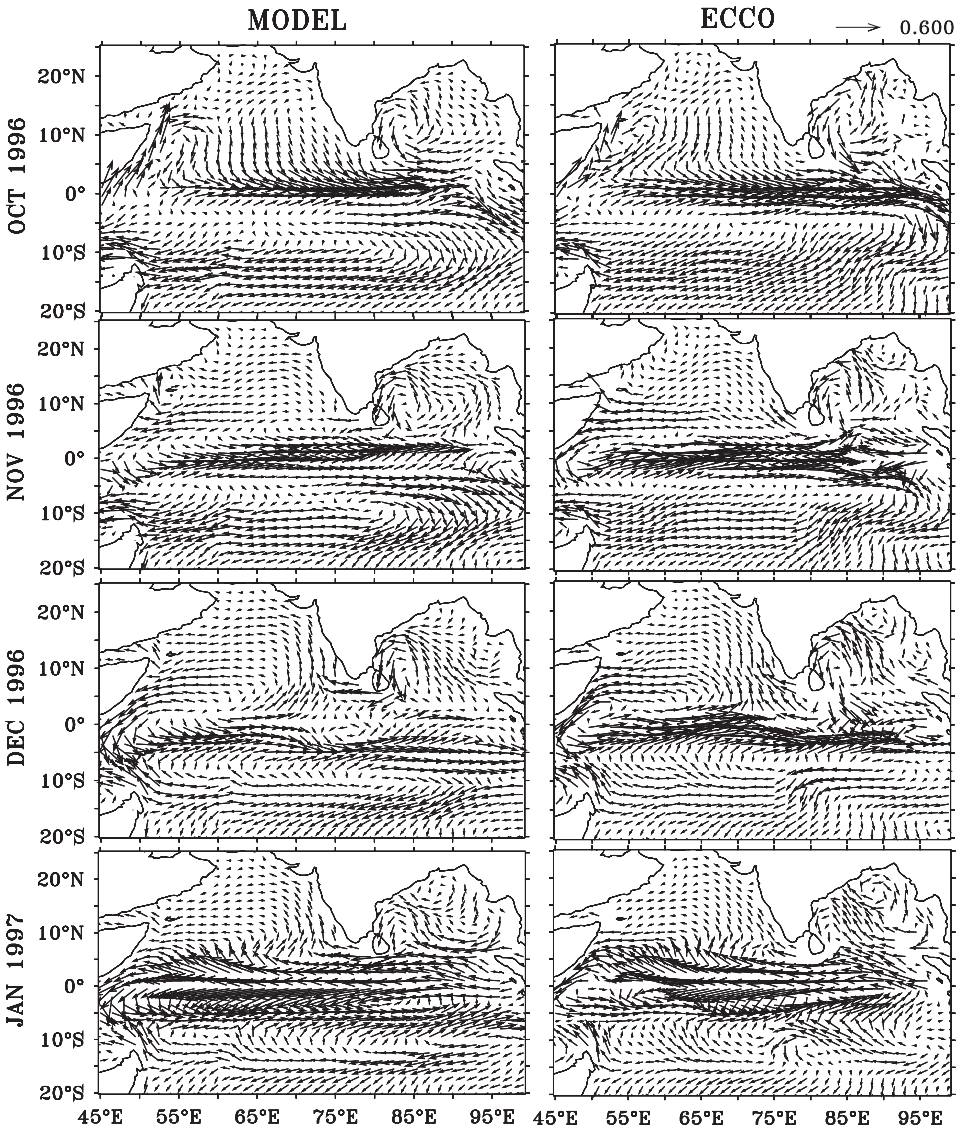

Figure 3. Surface currents (m/s) from 1996 October to 1997 January. Left panel shows model currents and right panel ECCO currents.

reducing the transport of warm water from the equatorial Indian Ocean to the STIO. In the case of the negative IOD year 1996, strong eastward surface currents are seen in the EIO and strong downwelling occurred east of 85E. By November, a clear narrow vertical circulation (vertical cell) is seen in the belt 90-95E. The strong Wyrtki Jet during this period induces downwelling in the region west of 93E. In fact, this result leads to the

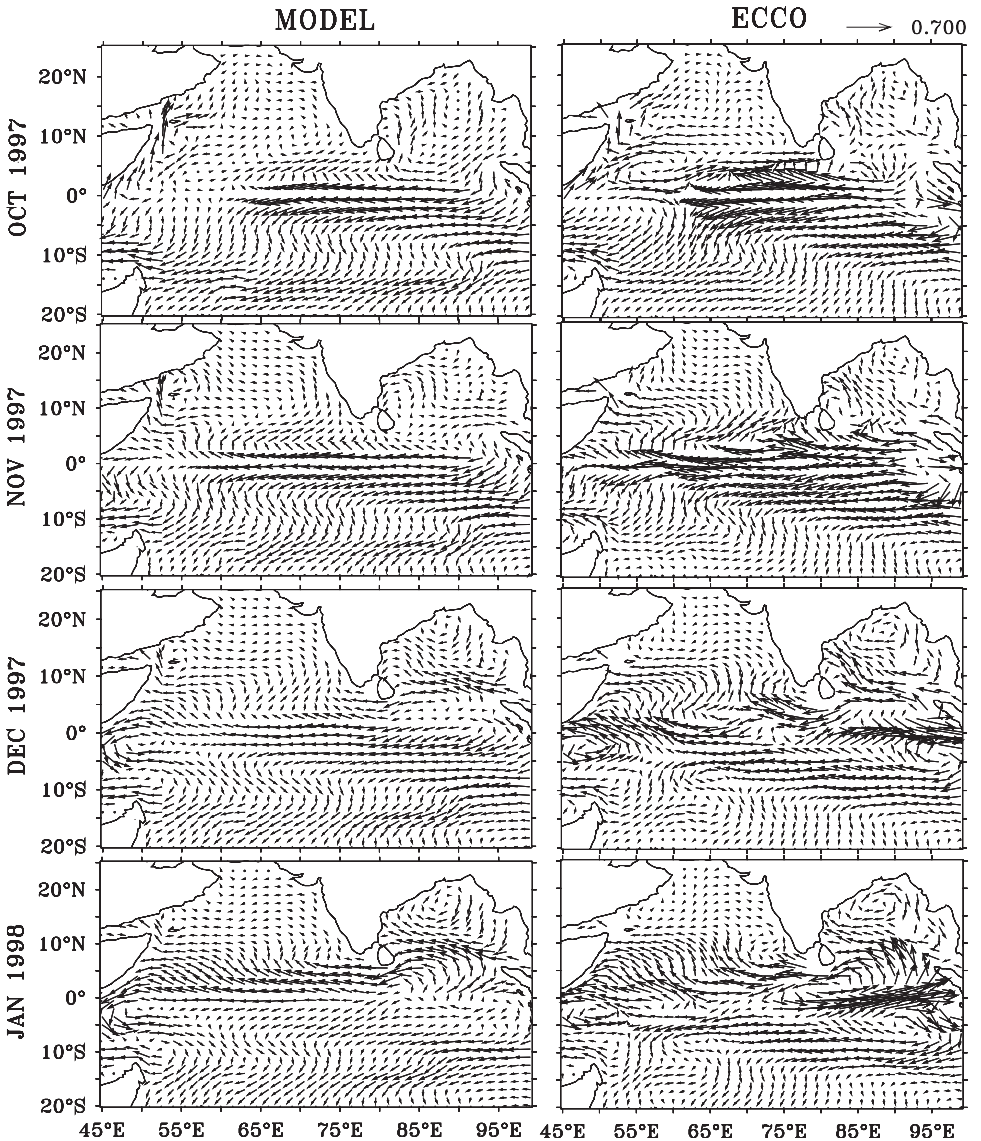

Figure 4. Same as Figure 3, but from October 1997 to January 1998.

development of a narrow vertical circulation during November. The entire eastern EIO (east of 80E) is marked by strong upwelling during December 1996. Similar features are observed in other negative IOD years also. During the negative IOD year 1996, negative vertical velocity anomalies are seen in the eastern EIO, and positive anomalies are seen in the western part (Fig. 8).

Earlier studies by Vinayachandran *et al.* (1999b, 2002), and Masson *et al.* (2002)

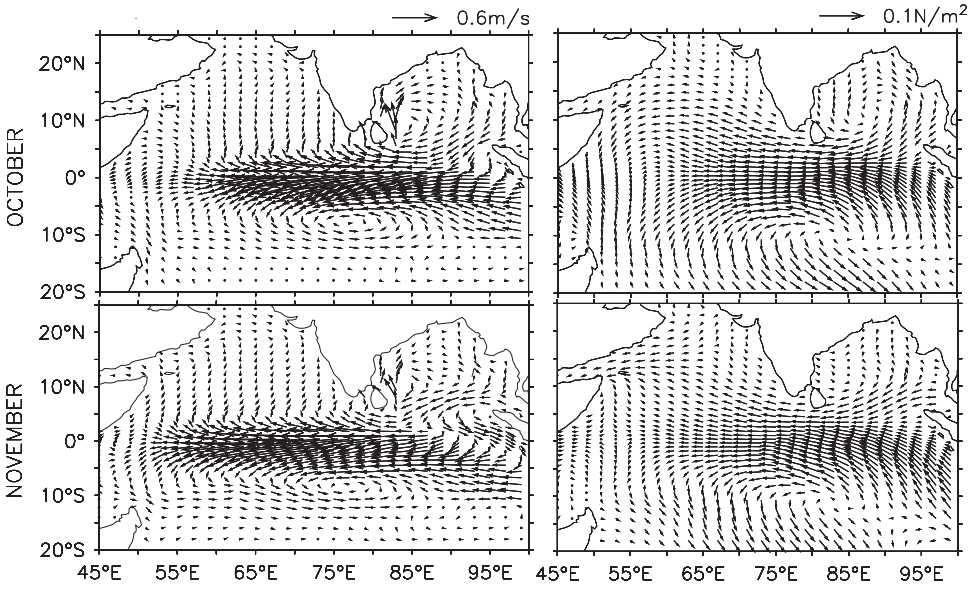

Figure 5. Anomaly composites of surface current (left) in m/s and wind stress (right) in N/m^2 during October and November. Composites are made for IOD years 1961, 1994 and 1997.

observe that the anomalous westward wind stress is mainly responsible for the weakening or reversal of the Wyrtki Jets during the IOD years. Grodsky *et al.* (2001) find a linear balance between local acceleration ($\partial u/\partial t$), zonal pressure gradient [$g(\partial\eta/\partial x)$] and zonal wind stress ($\tau^x/\rho H$) within the near surface equatorial zonal momentum in the Indian Ocean. The near surface zonal momentum balance can be expressed as

$$\frac{\partial u}{\partial t} = -g\frac{\partial \eta}{\partial x} + \frac{\tau^x}{\rho H} - au$$

where H is the vertical mixing length scale, g is the acceleration due to gravity of earth, η is the sea surface height anomaly, τ^x is the zonal wind stress, ρ is the density of sea water and last term 'au' is Rayleigh friction. A detailed description of momentum balance calculation is given in Grodsky *et al.* (2001). The anomalies of zonally averaged local acceleration, wind stress force, and pressure gradient force along the equator is shown in Figure 9. Anomalous wind and pressure gradient forcings are observed during the IOD years. The anomalous local zonal acceleration, especially during strong IOD years, is observed to be in phase with the wind forcing and is consistent with the findings of Grodsky *et al.* (2001). The momentum budget analysis shows that an imbalance between anomalous wind stress and pressure gradient force is observed during the recent, strongest positive IOD years 1961, 1994, and 1997 and during the negative IOD year 1996. This finding further supports that variability in the EIO circulation is primarily induced by the anomalous wind stress forcing during IOD years.

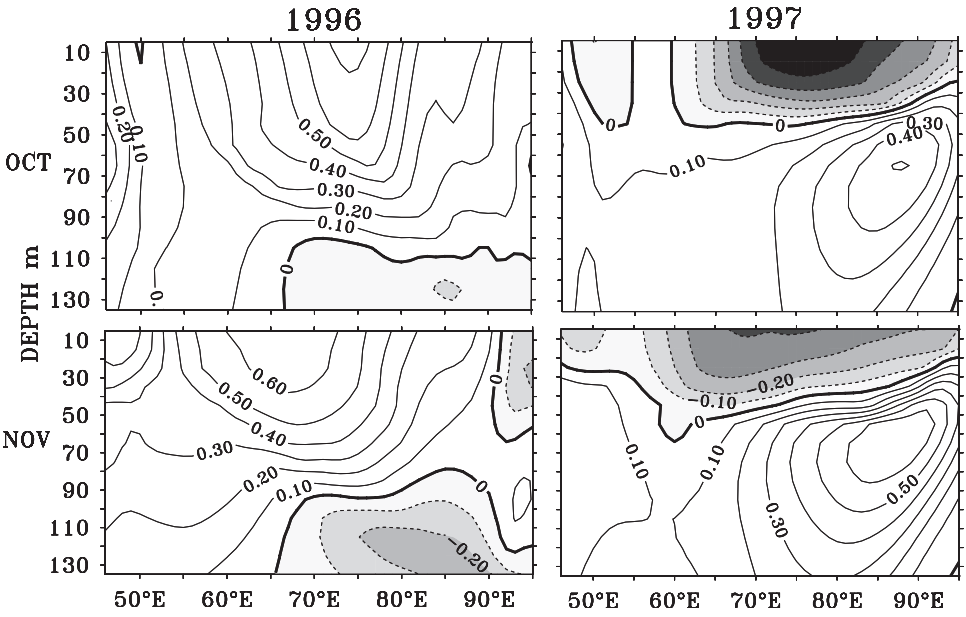

Figure 6. Zonal component of model Current (m/s) along the equator for 1996 and 1997. Shaded portion represents westward currents.

d. Anomalous Bay of Bengal circulation

The surface circulations in the Bay of Bengal are widely described in Schott and MacCreary (2001), Shankar *et al.* (2002) and Vinayachandran *et al.* (1999b). During late September, the East Indian Coastal Current (EICC) changes its direction (which normally flows northward north of 10N and southward south of 10N during southwest monsoon) and flows southward along the east coast of India. Satellite observations (Topex/Poseidon) show a cyclonic circulation in the central Bay of Bengal during November (Schott and MacCreary, 2001). In normal years during September to November, the southern BoB is characterised by an eastward flow and a southeastward flow along the east coast of Sri Lanka. In contrast, during positive IOD years, strong northward currents are observed (Fig. 4), and the eastward flow is either weak or is absent in the southern bay. Meanwhile, strong southwest flow dominates the eastern and southern bay. This is evident in both model simulations and in the ECCO datasets during all the positive IOD years. This southwestward flow and the southwest monsoon currents join southeast of Sri Lanka and feed the northward flow along the east coast of Sri Lanka. This result leads to the development of an anticyclonic circulation in the Bay of Bengal. During November, the westward flow in the southern bay extends further westward up to Sri Lanka, and by December, it extends up to about 75E. The climatological cyclonic circulation either vanishes or weakens and shifts towards the northwest bay during the positive IOD years. The similar features are seen in other positive IOD years also except during 1967. In 1967, the anticyclonic circulation in

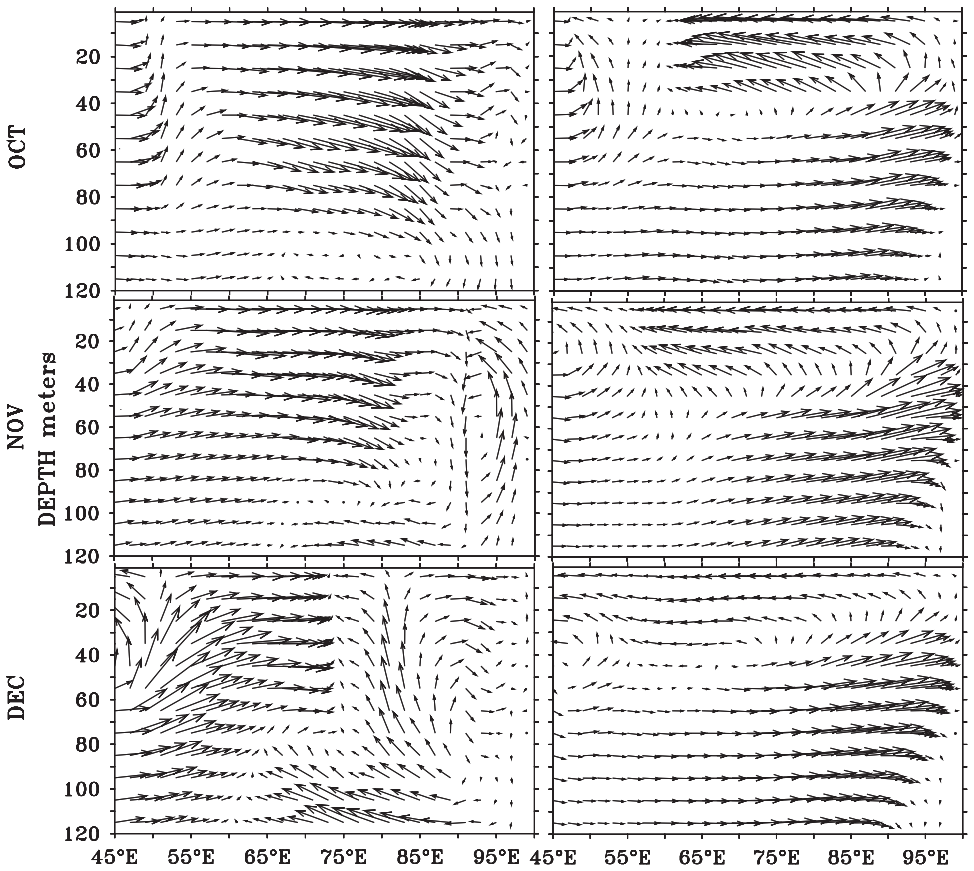

Figure 7. Zonal-Vertical current vectors from model simulation, October to December - 1996 (left panel) and 1997 (right panel). (Vertical velocity scaled up by 10^4).

the bay is not as disturbed. The anomalous northward flow during positive IOD years was replaced by a northeastward flow during 1967. However, during the negative dipole year 1996, the climatological circulation pattern is maintained in BoB with higher magnitudes (Fig. 3). Usually an anticyclonic eddy forms in the head bay in January. In contrast, during the positive dipole years, the anticyclonic circulation in the southern bay helps the northern gyre to form in November and December. The analysis of meridional vertical current along 90E establishes the contrasting features in the BoB circulation during the boreal fall of 1996 and 1997 (Fig. 10). Strong downwelling is observed south of 5N during October-November 1996, and northward currents are seen north of 5N. Strong upwelling is observed in the region between 2.5N and 5N by December 1996. However during 1997, strong upwelling is observed near the equator. During October and November 1997, the intense southward currents are seen south of 12.5N, which leads to surface upwelling south of equator. These southward currents are seen up to 50 m. Strong upwelling currents are

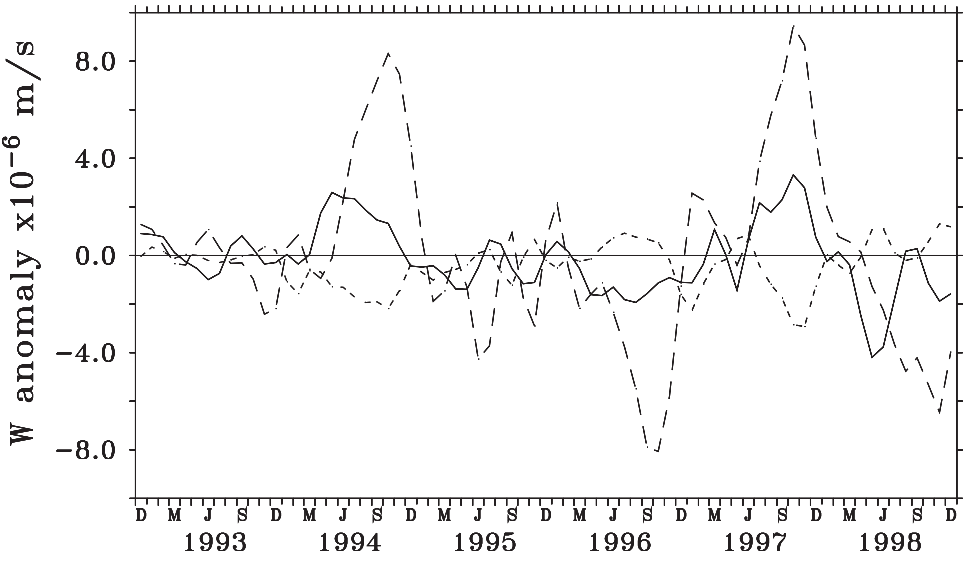

Figure 8. Vertical velocity anomalies at 50m from model averaged for the regions: 90E-110E, 10S-equator (Continuous line), 50E-75E, 10S-equator (dotted line) and 75E-90E, equator-5N (dashed line).

seen below 50 m in the region south of 15N. During December 1997 northward currents are observed between 5N and 13N instead of the climatological southward current, but the currents are southward in the region north of 13N. The anomalous southward currents during the boreal fall 1997 (positive IOD year) show the intrusion of low salinity BoB water to the central EIO.

e. Simulation of sea surface salinity

The sea surface salinity differences between the seasonal climatologies of the model and Levitus (1998) are shown in Figure 11. The seasonal climatologies show RMS differences

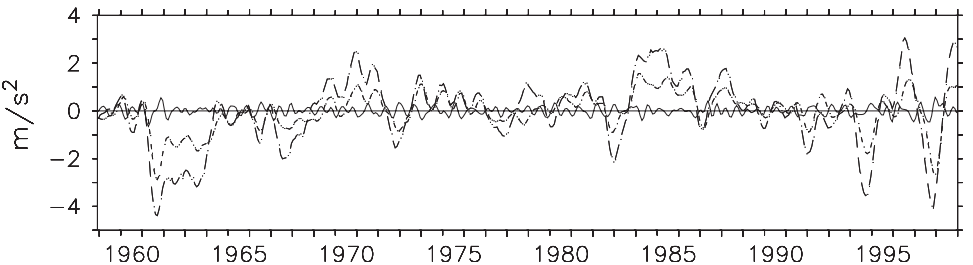

Figure 9. The anomalies of zonally averaged (50E to 90E) local acceleration (continuous line), pressure gradient force (dotted line) and wind stress force (dashed line) along the equator. All values are multiplied by 10^7.

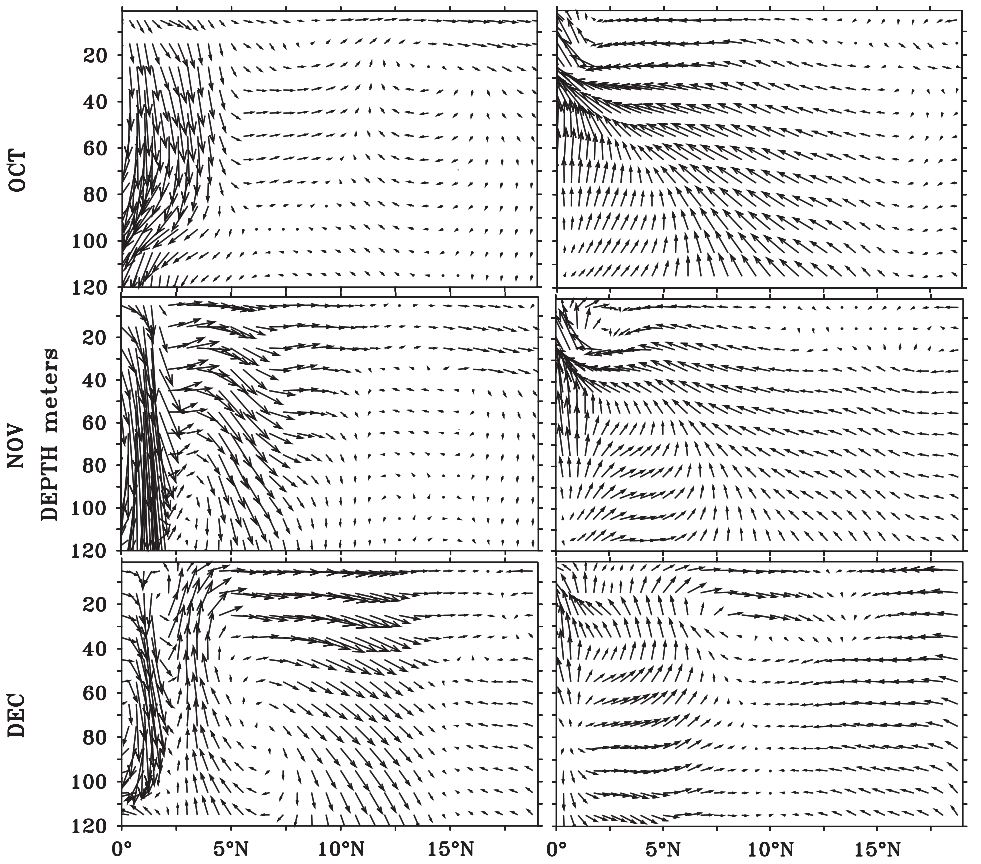

Figure 10. Meridional-Vertical section of currents along 90E from model during October to December 1996 (left panel) and 1997 (right panel). (Vertical velocity scaled up by 10^4).

of 0.30, 0.31, 0.32 and 0.36 respectively during December-February (DJF), March-May (MAM), June-August (JJA) and September-November (SON). The difference between model and observation is more in the head bay region and east coast of India, where the excess rainfall and freshwater discharge from rivers reduce the salinity of the sea water to the lowest within the Indian Ocean. The difference is seen to be about 0.6 in the southeastern Arabian Sea during DJF. In the eastern equatorial Indian Ocean, where a thick barrier layer exists during MAM and SON, the difference in SSS is less than 0.2 during all the seasons except SON (0.6 during SON). The vertical salinity stratifications in the equatorial region can intensify the surface and subsurface temperature anomalies (Masson *et al.*, 2004). In this context, it will be more relevant to understand the accuracy of the model simulation in this region. Vertical sections showing the difference between the seasonal climatologies of the model and Levitus (1998) for salinity averaged between 5S and 5N are shown in Figure 12. The model showed very good skill in salinity simulation

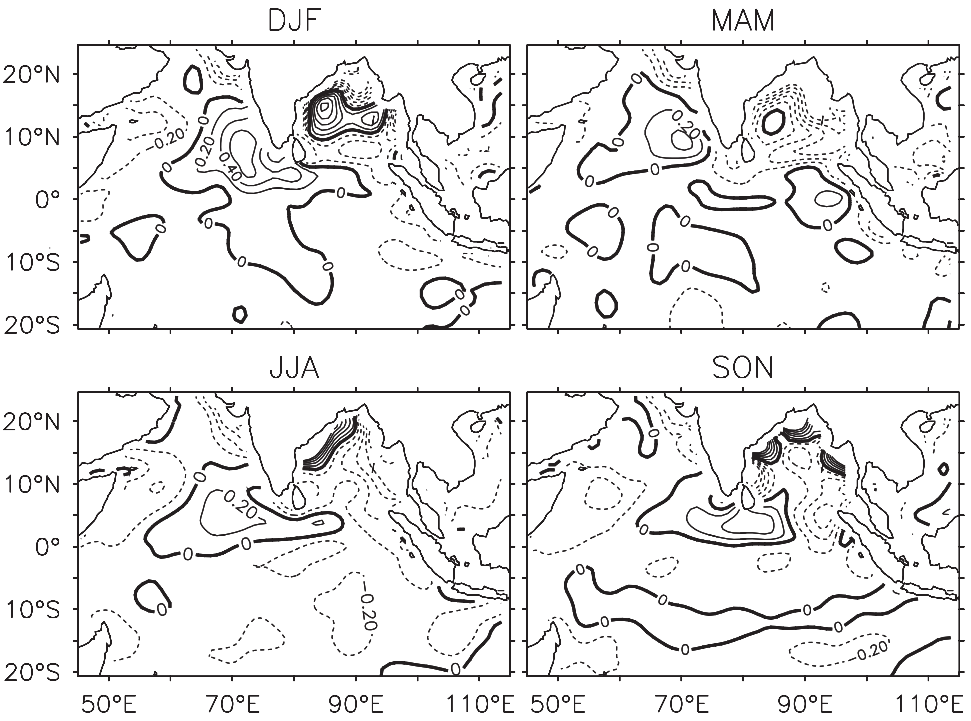

Figure 11. Sea surface salinity difference between seasonal climatologies of model and Levitus for December-February, March-May, June-August and September-November.

over this region. In the eastern EIO the difference between model and observations is less than 0.25 except during boreal fall (SON). During SON, the difference is 0.4 in the eastern EIO. The model accuracy in the salinity simulation is worth mentioning in the context of studying the interannual variability of salinity structure and establishing the possible relationship between salinity anomalies and the barrier layer formation.

f. Interannual variability of salinity in the Equatorial Indian Ocean

The composite of model SSS anomalies for the positive IOD years (1961, 1963, 1967, 1972, 1982, 1994, and 1997) and negative IOD years (1958, 1960, 1975, 1984, 1992, and 1996) are shown in Figure 13. The SSS pattern shows positive anomalies in the STIO during the positive IOD years. A maximum anomaly of about 1 is seen in the STIO. The negative SSS anomalies, which appear north of the equator in September around 90E spread further to the western parts of EIO by November. The composite SSS anomalies of about 0.2 for the positive IOD years 1961, 1994 and 1997 are observed in the western equatorial Indian Ocean (figure not shown). The maximum negative SSS anomalies are seen between 75E to 90E and from the equator to 5N. As discussed in the previous section during positive IOD years an anomalous anticyclonic circulation pattern exists in the Bay

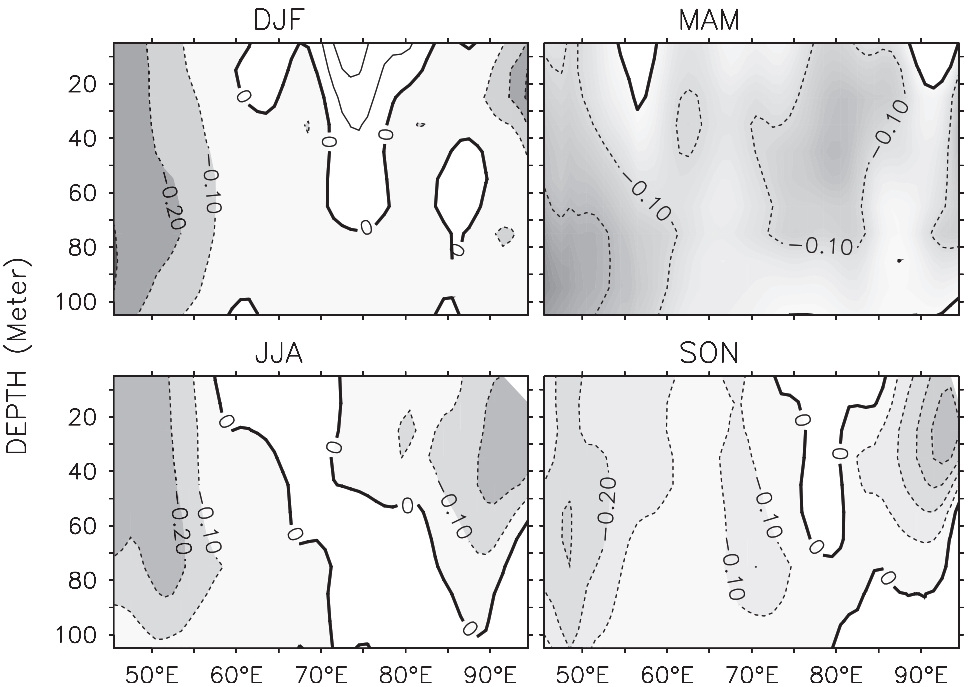

Figure 12. Zonal-Vertical section of salinity difference between the seasonal climatologies of the model and that of Levitus for December-February, March-May, June-August and September-November (5S-5N). Negative values are shaded.

of Bengal during October and November. The southwestward currents originating from the eastern bay bring low salinity water in to the central EIO, which leads to the reduction of salinity in this region. The advection of fresh Indian Ocean water from the eastern EIO by the westward currents also brings low salinity water into this region. In the STIO, the strong upwelling processes during positive IOD events contribute to the positive SSS anomalies. The modeled vertical velocity fields show positive anomalies in the central EIO, which are seen to be stronger than the anomalies in the STIO (Fig. 8). This further supports the theory that the advection of low salinity water from the east EIO and Bay of Bengal is responsible for the negative SSS anomalies in the central EIO between 75E and 90E. During the negative IOD years, negative SSS anomaly is observed in the STIO. A negative SSS anomaly of 0.8 is observed during October 1996. However considerable variability in SSS is not observed in the western equatorial Indian Ocean. Maximum positive SSS anomaly is observed in the central EIO east of 75E, which moves to the eastern BoB during October and November. Strong eastward currents (Wyrtki Jets) during the negative IOD years are responsible for this shifting of positive SSS anomalies. Thus the intrusion of high salinity water from the western EIO to the eastern BoB occurs in the negative IOD years due to the presence of the strong Wyrtki Jet.

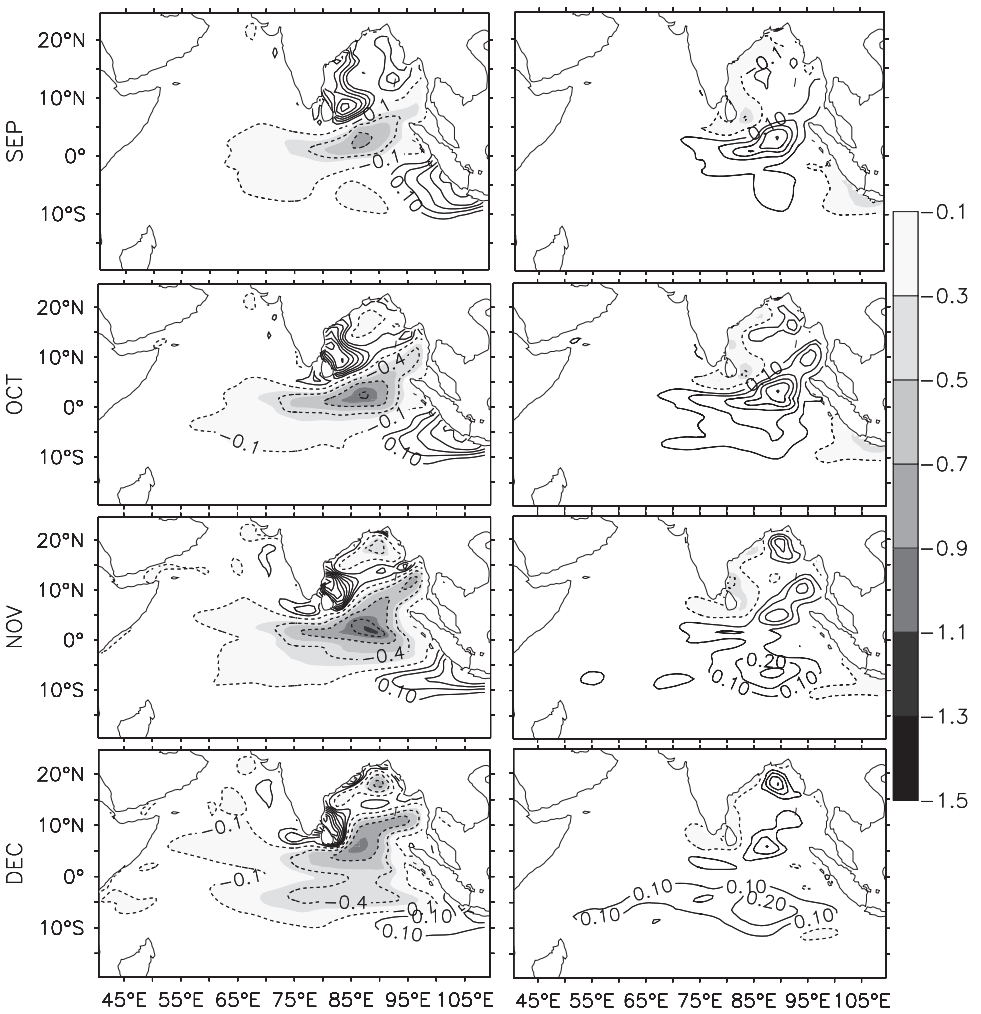

Figure 13. Composite of model sea surface salinity anomalies during September-December for positive IOD years (left panel) and negative IOD years (right panel). Negative values are shaded.

The variability in the salinity is not only limited to the surface, the subsurface salinity also shows considerable amount of interannual variability. The vertical structure of salinity anomaly composites for positive IOD years, from September-October averaged between 5S and 5N is shown in Figure 14. During the positive dipole years, the positive salinity anomalies persist in the east EIO. The maximum anomalies are observed at about 40 m. Weak negative anomalies are seen west of 90E. The negative salinity anomalies in the central EIO extends to a maximum depth of 80 m. Meanwhile the positive anomalies in the eastern EIO are observed up to 150 m during all the positive IOD years. These subsurface salinity patterns further support that the observed positive salinity anomaly east of 90E is

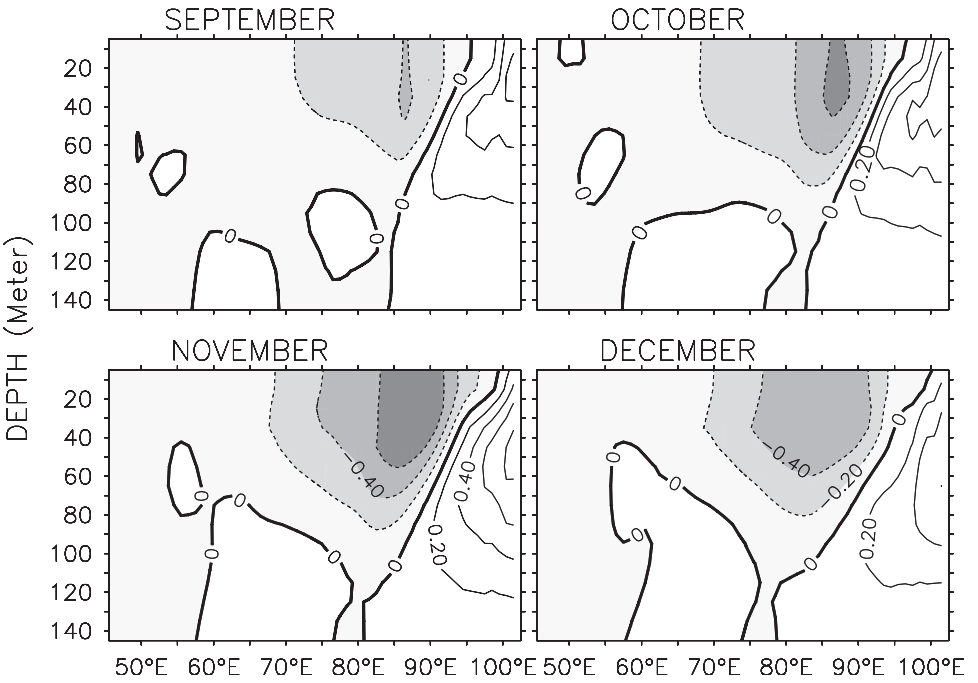

Figure 14. Zonal-Vertical section of model salinity anomalies from September-December, composite of positive IOD years. Negative anomalies are shaded.

caused by strong upwelling processes and the negative anomaly seen west of 90E is caused by the advection of upper ocean water from eastern EIO and Bay of Bengal. During the negative IOD years, even though the anomaly pattern reverses its sign, the magnitude is much weaker than the positive IOD years (figure not shown). During both the positive and negative dipole years, the salinity anomalies in the STIO are observed at deeper levels than in the central EIO.

The analysis of the long-term model SSS reveals that the variations in SSS over the STIO and central EIO (between 80E and 90E) are high during all dipole years, which is evident in the composite analysis also. A simple time series called Zonal Salinity Index (ZSI) is defined (to quantify the temperature variation) as the difference between the SSS anomalies of 90E to 105E, 10S to Equator and that of 80E to 90E, 5S to 5N to understand the variability in the SSS. The ZSI normalised by its standard deviation is given in Figure 15 (black line). Strong positive IOD years 1961, 1963, 1967, 1972, 1982, 1994 and 1997 are well represented by this index. However, ZSI does not represent the negative IOD events. During the positive IOD years, central EIO shows SSS anomalies about 1.7, but the SSS anomalies are less than 0.5 during negative IOD years over this region. The subsurface ZSI derived from the model at a depth of 50 m is shown in Figure 15 (dashed line). The subsurface ZSI shows a similar pattern as seen in the surface. Since the salinity anomalies

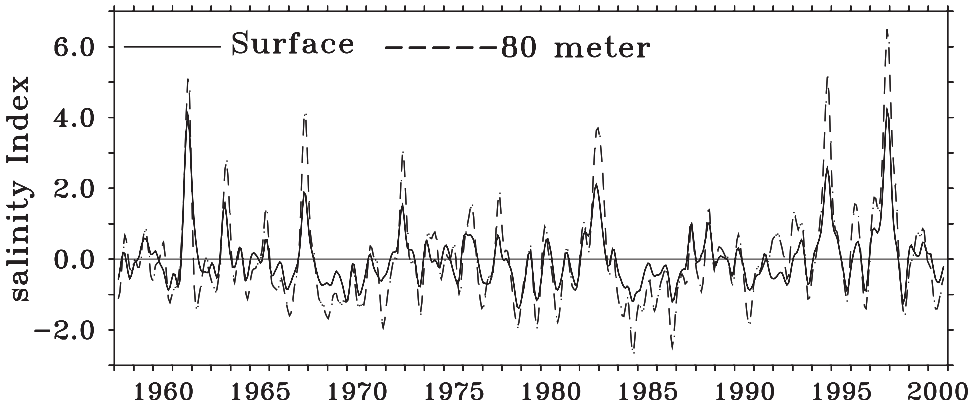

Figure 15. The difference between the model salinity anomalies averaged over 90E to 105E, 10S to Equator and 80E to 90E, 5S to 5N at surface (continuous line) and at 80m depth (dashed line).

are larger in the subsurface, ZSI shows higher values than the surface zonal salinity index. Also, Figure 15 illustrates that ZSI can be considered as a proxy for indicating the intensity of positive IOD events and also it manifests the anomalous upper ocean salinity transport between EIO and BoB during the IOD years.

For a better understanding of the oceanic processes contributing toward salinity anomalies in the central EIO (80E to 90E, equator to 5N) the upper ocean (50 m) salinity budget analysis has been performed. The salinity budget is calculated as follows:

$$\frac{\partial S}{\partial t} = -u\frac{\partial S}{\partial x} - v\frac{\partial S}{\partial y} + w\frac{\partial S}{\partial z} + (EMP)\bar{S} + \frac{\partial}{\partial z}\left(k\frac{\partial S}{\partial z}\right)$$

The individual contributions from zonal advection, meridional advection, vertical advection, evaporation minus precipitation (EMP) and vertical diffusion along with salt content rate ($\partial S/\partial t$) for the recent strongest positive IOD years 1961, 1994, and 1997 and the negative IOD year 1996 are shown in Figure 16. Negative salt content tendency during positive IOD years and positive salt content tendency during the negative IOD year 1996 are observed in the central EIO. However, the positive anomaly found in the negative IOD year is marginal. During the positive IOD years the zonal and meridional advection of fresh water contributes towards the decrease in the upper ocean salinity. The horizontal advection of low salinity water from the east EIO fresh pool, and BoB leads to the reduction of upper ocean salinity during these anomalous years. The zonal advection of fresh water from eastern EIO is observed as the major contributor for the negative salinity anomaly. Meanwhile the vertical advection and vertical diffusion components contribute to increase the salinity. The analysis shows that the contribution from EMP is much less in the central EIO. During the negative IOD year 1996, the zonal advection of high salinity water from western Indian Ocean appears to be the sole factor responsible for the increase in upper ocean salinity. Meridional advection, vertical advection and vertical diffusion

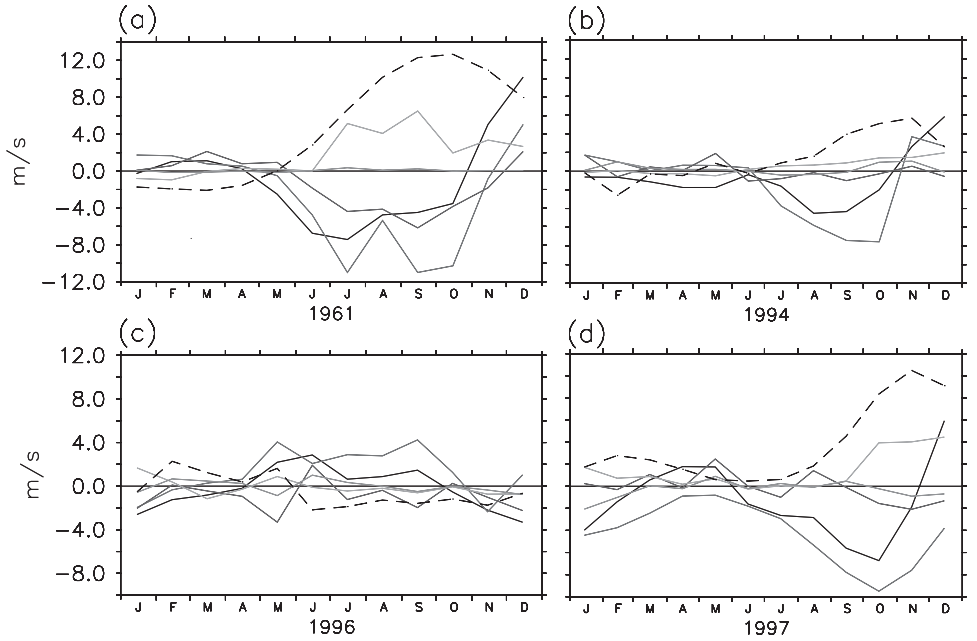

Figure 16. Anomalies of model 50m salt content tendency (black line), vertical advection (green line), meridional advection (blue line), zonal advection (red line), vertical diffusion (dashed line) and evaporation minus precipitation (purple line) in the region 80E to 90E, equator to 5N for 1961 (a), 1994 (b), 1996 (c) and 1997 (d). All values are multiplied by 10^6.

components act to decrease salinity. The contribution from vertical advection and EMP are relatively small compared to the horizontal advection and diffusive terms.

g. Barrier layer thickness anomalies

In the tropical Indian Ocean, the largest anomalies in the barrier layer thickness are observed in the eastern equatorial Indian Ocean during the dipole mode events. During positive IOD years, the reduced precipitation and strong upwelling induced by anomalous westward currents erode the barrier layer in the eastern EIO. The eastern EIO shows negative BLT anomalies of about 40 m during November and December, which shows the complete collapse of the barrier layer (Fig. 17). This negative BLT anomaly extends up to 70E in the equatorial region. Surrounding the negative anomaly region, a band of positive BLT anomaly is seen centered around 55E at equator extending towards both hemispheres. These positive anomalies show a maximum of about 15 m in the composites during November. During the negative IOD years, positive BLT anomalies (about 10 m during November and December) are present in the east EIO. These BLT anomalies show strong interannual variability during the IOD years. In November 1996 positive BLT anomalies of about 40 m are observed in the eastern EIO. However negative BLT anomalies of less than

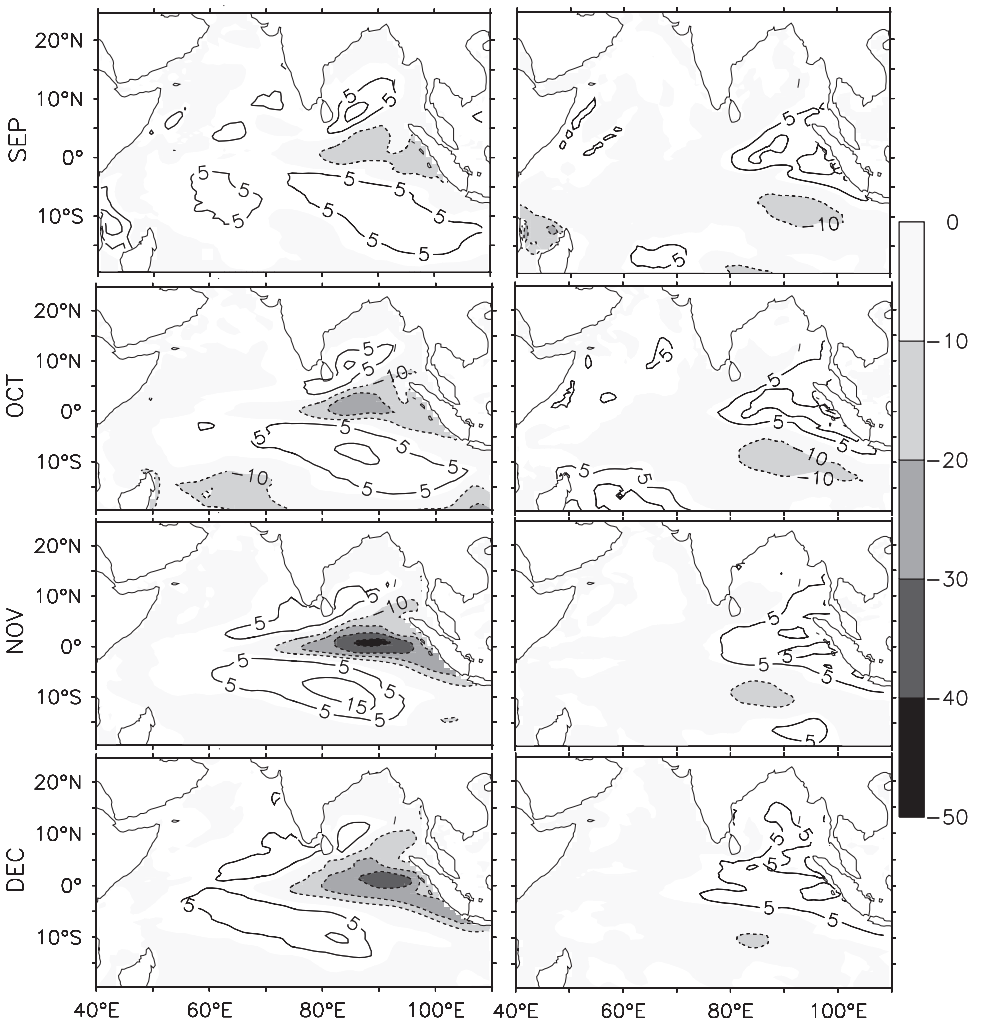

Figure 17. Composite of barrier layer thickness anomalies during September to December for positive IOD years (left panel) and negative IOD years (right panel). Negative anomalies are shaded.

15 m are observed in the western tropical Indian Ocean. The BLT anomalies are stronger in the eastern EIO during both positive and negative IOD events. The observed cooling (warming) during positive (negative) IOD events is also more intense in the eastern basin than the western warming (cooling). This suggests that the intensification or weakening of the barrier layer in the equatorial Indian Ocean is critical in the survival or strengthening of surface and subsurface temperature anomalies associated with the IOD events.

The barrier layer formation and thickening are controlled by the strong haline stratifica-

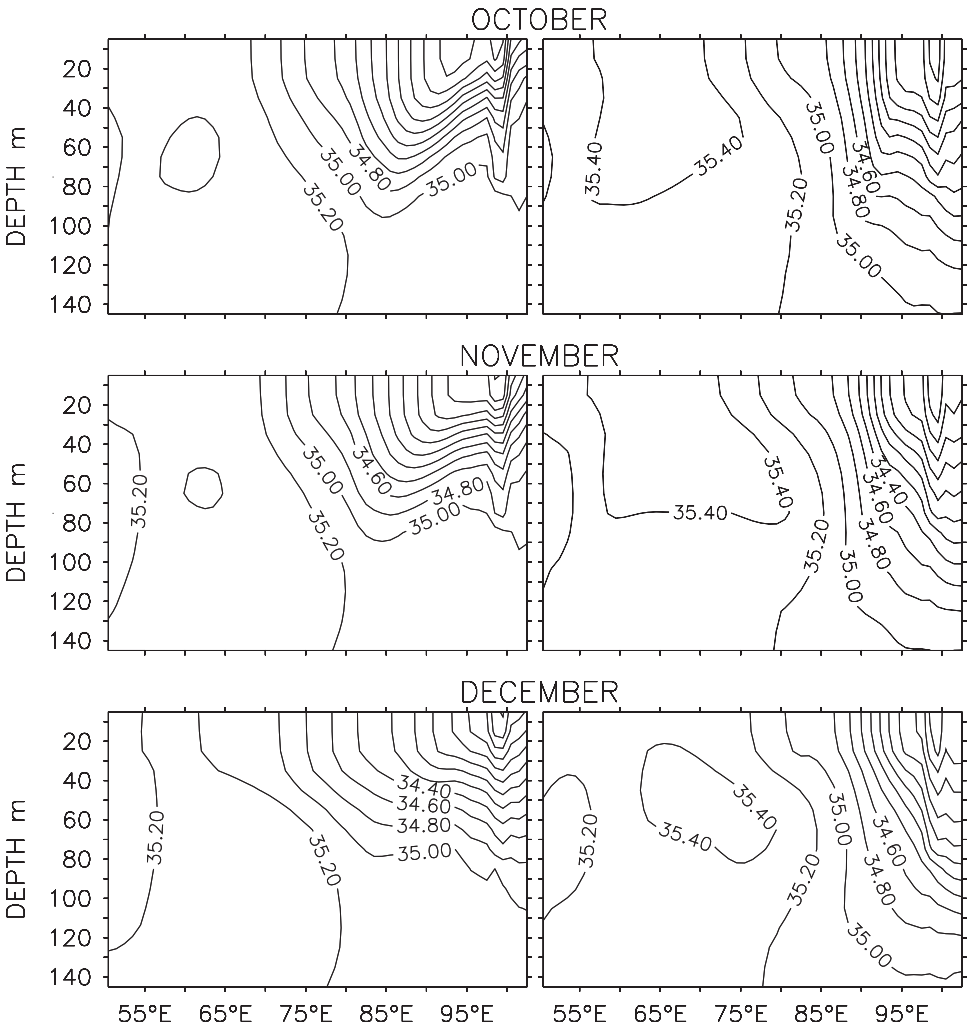

Figure 18. Zonal-Vertical section of model salinity composite from October to December (5S-5N) for positive IOD years (left panel) and negative IOD years (right panel).

tions in the upper ocean. The vertical salinity distribution along the equatorial section (average of 5S-5N) shows stratification within a depth of 40-50 m in the eastern part during the positive IOD years (Fig. 18). However, central EIO shows salinity stratification up to a depth of about 80 m in the composites. In the case of the negative dipole years, strong salinity stratification is seen up to 150 m in the eastern EIO. But no such vertical haline structure is observed in the western EIO during both positive and negative IOD years. The strong salinity stratification in the eastern EIO helps to trap the momentum flux in the upper mixed layer and warms the ocean through the formation of stable thick barrier layers. The

salinity stratification in the EEIO shows strong variability between positive and negative IOD years. The intensification or weakening of salinity stratification in the EEIO is the main factor, which drive the strong temperature variabilities during IOD events through strong BLT anomalies. The less marked salinity stratification is responsible for the weak temperature anomalies in the western EIO.

Salinity anomalies exhibit an inverse relationship with temperature anomalies and BLT anomalies. This is evident in the Hovmoller diagram for SST, SSS and BLT anomalies (Fig. 19). For instance, positive SSS anomalies are observed in the STIO during 1994 and 1997 prior to the appearance of eastern cooling. Further analysis revealed that similar types of features are seen in the subsurface (50 m) also (figure not shown). The positive (negative) salinity anomalies are associated with decrease (increase) in BLT. As discussed in the previous sections, the changes in the circulation pattern over the equatorial Indian Ocean and Bay of Bengal are responsible to a large extent for salinity changes in the central EIO. The weakening of subsurface salinity stratifications causes decrease in BLT in the STIO and leads to strong cooling through entrainment mixing. During all the IOD years, the SSS anomalies are able to represent the variability in the BLT. However, during 1996, the salinity anomalies are not evident in the subsurface as observed in the positive IOD years.

4. Conclusions

The Indian Ocean dipole mode denotes a dominant mode of basin scale SST variability in the tropical Indian Ocean. A well parameterized Ocean General Circulation model MOM4 has been used to simulate the surface and subsurface features associated with the IOD events. The model simulations were validated with observations and found comparable with SODA and ECCO data sets. The model seasonal SST, current and salinity, all reproduced the observed climatological features in the Indian Ocean. In this study, the seasonal climatologies of the model and that of Levitus (of SSS) showed an RMS difference of 0.30, 0.31, 0.32 and 0.36 for DJF, MAM, JJA and SON, respectively. During the positive IOD years, north equatorial currents weaken and are confined to a narrow band and disappear near Sri Lanka. However, during the negative IOD year 1996, the southwest monsoon current is intense. In the normal years, the southern BoB is characterised by an eastward flow and southeastward flow along the east coast of Sri Lanka. In contrast, during the positive IOD years, the strong northward currents are observed in the region. The eastward flow either weakens or disappears from southern bay. During the positive dipole years, positive SSS anomalies are seen in the STIO and negative SSS anomalies are seen north of the equator (west of 90E). The maximum negative SSS anomalies are seen between 75E to 90E and equator to 5N. The maximum salinity anomalies are seen at about 40 m during positive IOD years. The negative salinity anomalies, seen in the western equatorial Indian Ocean are less than the positive anomalies of the eastern region (both intensity and vertical extent). The barrier layer thickness anomalies are significantly higher in the eastern equatorial Indian Ocean during the dipole years. The barrier layer formation

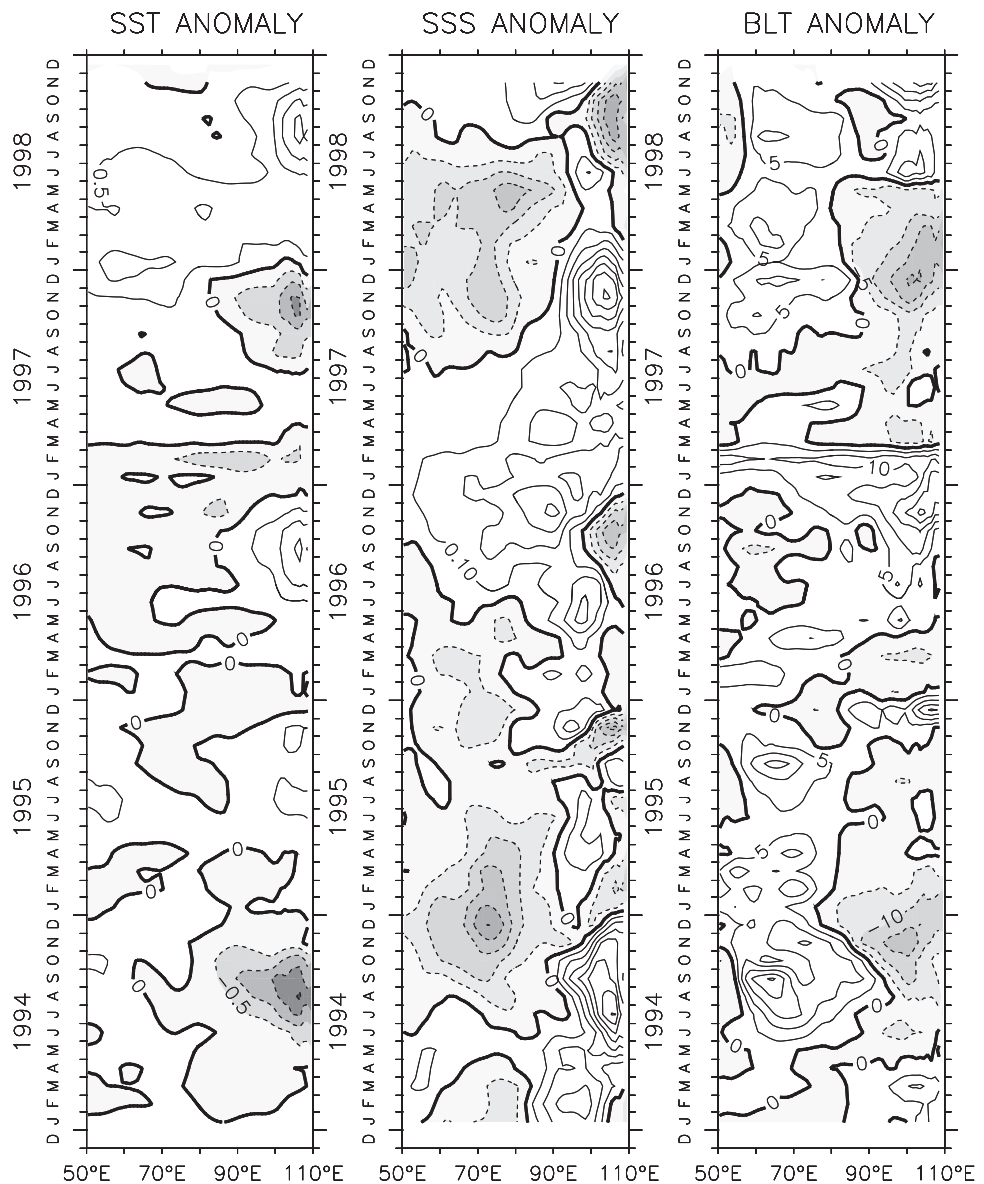

Figure 19. Anomalies of model SST (left panel), SSS (middle panel) and BLT (right panel) averaged for 10S-equator. Negative anomalies are shaded.

and thickening are controlled by the strong haline stratifications in the upper ocean. The absence of salinity induced barrier layer in the eastern equatorial Indian Ocean during positive IOD years enhanced the entrainment cooling and this further lead to an anomalous (negative) SST pattern in the region. The upwelling of high salinity subsurface water

weakens the barrier layer in the southeastern equatorial Indian Ocean during positive IOD events. The salinity anomalies exhibit an inverse relationship with the temperature and BLT anomalies.

Acknowledgments. Bijoy Thompson acknowledges CSIR, India for JRF/SRF fellowship. The financial support from the Department of Ocean Development, Govt. of India is acknowledged. The authors acknowledge Dr. Stephan Griffies and Dr. P. S. Swathi for their support and discussions during model installation and integration. Acknowledgments are also due to GFDL for making the MOM4 code available, NCAR, BADC, UMD, and ECCO for their data sets. The encouragement and support from Director, IITM is acknowledged. We thank Dr. Peter Mayes and Mark R Jordan II for reading the manuscript and for their suggestions. The comments from two anonymous reviewers helped to improve the manuscript.

REFERENCES

Annamalai, H., S. P. Xie, J. P. McCreary and R. Murtugudde. 2003. Coupled dynamics over Indian Ocean: Spring initiation of the Zonal Mode. Deep-Sea Res. II, *50*, 2305–2330.

Behera, S. K., R. Krishnan and T. Yamagata. 1999. Unusual ocean-atmosphere conditions in the tropical Indian Ocean during 1994. Geophys. Res. Lett., *26*, 3001–3004.

Behera, S. K., J. J. Luo, S. Masson, P. Delecluse, S. Gualdi, A. Navarra and T. Yamagata. 2005. Paramount impact of the Indian Ocean Dipole on the East African short rains: A CGCM study. J. Climate, *18*, 4514–4530.

Behera, S. K., P. S. Salvekar and T. Yamagata. 2000. Simulation of interannual SST variation in the tropical Indian Ocean. J. Climate, *13*, 3487–3489.

Behera, S. K. and T. Yamagata. 2003. Impact of the Indian Ocean dipole on the southern oscillation. J. Meteorol. Soc. Japan., *81*, 169–177.

Carton, J. A., G. Chepurin, X. Cao and B. S. Giese. 2000. A simple ocean data assimilation analysis of the global upper ocean 1950–1995, Part 1: methodology. J. Phys. Oceanogr., *30*, 294–309.

Carton, J. A., B. S. Giese and S. A. Grodsky. 2005. Sea level rise and the warming of the oceans in the Simple Ocean Data Assimilation (SODA) ocean reanalysis. J. Geophys. Res., *110*(C9), C0900610.1029/2004JC002817.

Godfrey, J. S., E.F. Bradle, P. A. Coppin, L. Pender, T. J. McDougall, E.W. Schulz and I. Helmond. 1999. Measurements of upper ocean heat and freshwater budgets near a drifting buoy in the equatorial Indian Ocean. J. Geophys. Res., *104*(C6), 13,269–13,302.

Griffies, S. M., M. J. Harrison, R. C. Pacnowski and A. Rosati. 2003. A Technical Guide to MOM4, GFDL Ocean Group Technical Report No. 5, Princeton, NJ: NOAA/Geophysical Fluid Dynamics Laboratory.

Grodsky, S. A., J. A. Carton and R. Murtugudde. 2001. Anomalous surface currents in the tropical Indian Ocean. Geophys. Res. Lett., *28*, 4207.

Han, W., J. P. McCreary, D. L. T. Anderson and A. J. Mariano. 1999. On the dynamics of eastward surface jets in the equatorial Indian Ocean. J. Phys. Oceanogr., *29*, 2191–2209.

Hastenrath, S. and L. Greischar. 1991. The monsoonal current regimes of the tropical Indian Ocean: observed surface flow fields and their geostrophic and wind-driven components. J. Geophys. Res., *96*, 12619–12633.

Iizuka, S., T. Matsuura and T. Yamagata. 2000. The Indian Ocean SST dipole simulated in a coupled general circulation model. Geophys. Res. Lett., *27*, 3369–3372.

Jensen, T. G. 2006. Wind-driven response of the northern Indian Ocean to climate extremes. J. Climate (in press).

Kohl, A., D. Stammer, B. Cornuelle, E. Remy, Y. Lu, P. Heimbach and C. Wunsch. 2003. The Global 1° WOCE Synthesis: 1992–2001, The ECCO Report Series, Report No. 20.

Large, W.G. and S.G. Yeager. 2004. Diurnal to decadal global forcing for ocean and sea-ice models: the data sets and flux climatologies. NCAR, Technical Note NCAR/TN-460+STR, 111 pp.

Levitus, S. 1998. Climatological atlas of the world ocean, Tech. Rep., NOAA, Rockville, MD.

Masson, S., P. Delecluse, J. P. Boulanger and C. Menkes. 2002. A model study of the seasonal variability and formation mechanism of barrier layer in the eastern equatorial Indian Ocean. J. Geophys. Res., *107*(C12), 8017, doi:10.1029/2001JC000832.

Masson, S., C. Menkes, P. Delecluse and J. P. Boulanger. 2003. Impacts of the salinity on the eastern Indian Ocean during the termination of the fall Wyrtki jet. J. Geophys. Res., *108*(C3), 3067, doi:10.1029/2001JC000833.

Masson, S., C. Menkes, P. Delecluse and J. P. Boulanger. 2004. Impacts of salinity on the eastern Indian Oceans during termination of the fall Wyrtki jet. J. Geophys. Res., *109*, C02002, doi:10.1029/2003JC001807.

Murtugudde, R. and A. J. Busalacchi. 1999. Interannual variability of the dynamics and thermodynamics of the tropical Indian Ocean, J. Climate, *12*, 2300–2326.

Murtugudde, R., J. P. McCreary and A. J. Busalacchi. 2000. Oceanic processes associated with anomalous events in the Indian Ocean with relevance to 1997–1998. J. Geophys. Res., *105*, 3295–3306.

Nicholls, N. 1989. Sea Surface temperatures and Australian winter rainfall. J. Climate, *2*, 965–973.

Rao, R. R. and R. Sivakumar. 2003. Seasonal variability of seas surface salinity and salt budget of the mixed layer of the north Indian Ocean, J. Geophys. Res., *108*, C110.1029/2001JC000907

Rao, S. A. and S. K. Behera. 2005. Subsurface influence on SST in the tropical Indian Ocean: structure and interannual variability. Dyn. Atmos. Oceans, *39*, 103–135

Rao, S. A., S. K. Behra, Y. Masumoto and T. Yamagata. 2002a. Interannual subsurface variability in the tropical Indian Ocean with a special emphasis on the Indian Ocean dipole, Deep-Sea Res. II, *49*, 1549–1572.

Rao, S. A., V. V. Gopalakrishna, S. R. Shetye and T. Yamagata. 2002b. Why were cool SST anomalies absent in the Bay of Bengal during the 1997 Indian Ocean dipole event? Geophys. Res. Lett., *29*(11), 1555, doi:10.1029/2001GL014645.

Rayner, N. A., D. E. Parker, E. B. Horton, C. K. Folland, L. V. Alexander, D. P. Rowell, E. C. Kent and A. Kaplan. 2003. Global analyses of sea surface temperature, sea ice, and night marine air temperature since the late nineteenth century. J. Geophys. Res., *108*, D14, 4407, doi:10.1029/2002JD002670.

Reverdin, G. 1987. The upper equatorial Indian Ocean: the climatological seasonal cycle. J. Phys. Oceanogr., *17*, 903–927.

Saji, N. H., B. N. Goswami, P. N. Vinayachandran and T. Yamagata. 1999. A dipole mode in the tropical Indian Ocean. Nature, *401*, 360–363.

Saji, N. H. and T. Yamagata. 2003. Possible impacts of Indian Ocean dipole mode events on global climate. Climate Res., *25*, 151–169.

Schott, F. A. and J. P. MacCreary Jr. 2001. The monsoon circulation of the Indian Ocean. Prog. Oceanogr., *51*, 1–123.

Shaji, C., S. Iizuka and T. Matsuura. 2003. Seasonal variability of near-surface heat budget of selected oceanic areas in the north tropical Indian Ocean. J. Oceangr., 59, 37–103.

Shankar, D., P. N. Vinayachandran , A. S. Unnikrishnan and S. R. Shetye. 2002. The monsoon currents in the north Indian Ocean. Prog. Oceanogr., *52*, 63–119.

Sprintall, J. and M. Tomczak. 1992. Evidence of the barrier layer in the surface layer of the tropics. J. Geophys. Res., *97*, 7305–7316.

Vinayachandran, P.N., S. Iizuka and T. Yamagata. 2002. Indian Ocean dipole mode events in an ocean General Circulation model, Deep-Sea Res. II, *49*, 1573–1596.

Vinayachandran P. N., Y. Masumoto, T. Mikawa and T. Yamagata. 1999a. Intrusion of the southwest monsoon current into the Bay of Bengal. J. Geophys. Res., *104*(C5), 11,077–11,085.

Vinayachandran, P. N., N. H. Saji and T. Yamagata. 1999b. Response of the equatorial Indian Ocean to an unusual wind event during 1994. Geophys. Res. Lett., *26*(11), 1613.

Webster P. J., A. M. Moore, J. P. Loschnigg and R. R. Leben. 1999. Coupled ocean-atmosphere dynamics n the Indian Ocean during 1997–1998. Nature*, 401*, 356–360.

Zubair, L., S. A. Rao and T. Yamagata. 2003. Modulation of Sri Lankan Maha rainfall by the Indian Ocean dipole. Geophys. Res. Lett., *30*(2), 1063, doi:10.1029/2002GL015639.

Received: *14 February, 2006*; revised: *29 September, 2006*.